J Nanostruct 16(3): 3835-3844, Summer 2026

RESEARCH PAPER

Advanced Fabrication of Gold Nanoparticles via Laser Ablation and their Structure-Dependent Antibacterial Effect

*Rejwan K. Ibrahim [1], Wisam Jawad Obiad [2], Duaa. A. Mohameed [1], Noor M. Saadoon [3]**

[1] *Centre of Nanotechnology and Advanced Material, University of Technology, Iraq*

[2] *Department of Physiotherapy, College of Health and Medical Techniques, Al-esraa University, Iraq*

[3] *Science and Laser Technology Department, Applied Science Collage, University of Technology, Iraq*

ARTICLE INFO

Article History:
Received 16 March 2026
Accepted 25 June 2026
Published 01 July 2026

Keywords:
Antibacterial Activity
Gold Nanoparticles
Laser Ablation in Liquids
Nanostructure Characterization
Surface Plasmon Resonance

ABSTRACT

This research article focused on developing various green, inexpensive techniques to prepare and assess the characteristics of Au-NPs. Using a 1064 nm wavelength laser in conjunction with DW as a solvent to prepare the Au-NPs by means of a liquid PLAL process, both XRD and absorbance spectroscopy detected that the resulting particles were composed of elemental gold and possessed a face-centered cubic (fcc) crystal lattice structure. The fcc crystalline structure was also verified from the presence of an absorption peak indicating surface plasmon resonance (SPR) at 523 nm in the UV-visible absorption spectrum generated from the Au-NPs. The antibacterial activity of Au-NPs was observed via an inhibition zone and was due to the Au-NPs possessing a high surface area to volume ratio, thus enabling them to be better able to alter and/or kill E. coli and Staphylococcus aureus.

How to cite this article
Ibrahim R., Obiad W., Mohameed D., Saadoon M. Advanced Fabrication of Gold Nanoparticles via Laser Ablation and their Structure-Dependent Antibacterial Effect . J Nanostruct, 2026; 16(3):3835-3844. DOI: 10.22052/JNS.2026.03.070

INTRODUCTION

Rapid progress in both nanotechnology and nanomaterials has generated numerous research opportunities for investigating theranostic use of nanoparticles within molecular imaging. As such, gold nanoparticles have become a favored mechanism for performing molecular imaging due to their unique attributes including being a good source of contrast agent and carrier for drugs. Characteristics of gold nanoparticles that contribute to their popularity include their high chemical stability, ability to create covalent bonds with a wide range of molecules and their excellent compatibility with human cells. Many techniques exist for producing gold nanoparticles (traditional chemical synthesis, radiation-based, electrochemical, biological synthesis, and pulsed laser ablation in a liquid medium [1,2], and while there are multiple ways to fabricate gold nanoparticles, each has pros and cons associated with the respective process. Most frequently, pulsed laser ablation (PLA) in liquid is the general method used to manufacture nanoscale materials owing to the fact that the method is simple, inexpensive, efficient, and environmentally safe [3-5].

Gold nanoparticles can be produced via the laser ablation of a solid gold target submerged in a liquid medium. When the laser beam is directed at the solid gold target, the surface of the target heats up and melts due to localized heating from the beam. This primarily occurs

* *Corresponding Author Email: mae.visit.04@uotechnology.edu.iq*

by ejection/evaporation of the material from the surface of the target when atoms, clusters and/or droplets are released from the solid gold target. The released atoms, clusters and/or droplets cool down after their ejection creating the gold nanoparticles in the liquid medium [6;7]. Therefore both of the previously discussed processes create gold nanoparticles that are suspended in liquid (or an organic) medium. Also, since the PLAL method does not require the use of reducing agents or toxic surfactants, the resultant purity, quality and homogeneity of the produced nanoparticles is greater than would have been achieved using other methods. Due to the high purity and large, discrete, and contamination-free surfaces of the gold nanoparticles produced by using PLAL, the gold nanoparticles are an excellent surface for coupling to biocompatible polymers. After the AuNPs bind to the bacterial membrane, substances within the AuNPs will be released out of the outer membrane and peptidoglycan layer of the bacteria, resulting in death of the bacterium [8-10].

The PLAL mechanism includes a number of different physical mechanisms. The laser energy is absorbed by a metal target, in emitting a laser from a PLAL source; as the area receiving laser energy heats, it becomes photoionized. As the ablation laser converts energy to an excitaion of the electron bonding of the metal target (breaking bonds with enough energy), the electrons that have been released due to the breakage of bonds will absorb incoming laser photons and produce multiple ionizations of the target material through Inverse Bremsstrahlung [11-15]. In addition, there is a simultaneous explosive, vaporisation and boiling event. The metal targets will be ablated into liquid droplets, solid masses, plasma plumes and/or vapours. The area ablated will depend on the amount of energy absorbed.

MATERIALS AND METHODS

Preparation of Au nanoparticles

The most efficient and promising way to produce gold nanoparticles is through laser ablation. The laser ablation technique has been used to create many types of nanomaterials, and is touted as an environmentally sustainable method of producing gold nanoparticles. Researchers interested in producing gold nanoparticles via this type of production have taken advantage of the widespread availability and effectiveness of the Nd:YAG laser source. As an example, by placing 3 ml of deionized water above a gold pellet and

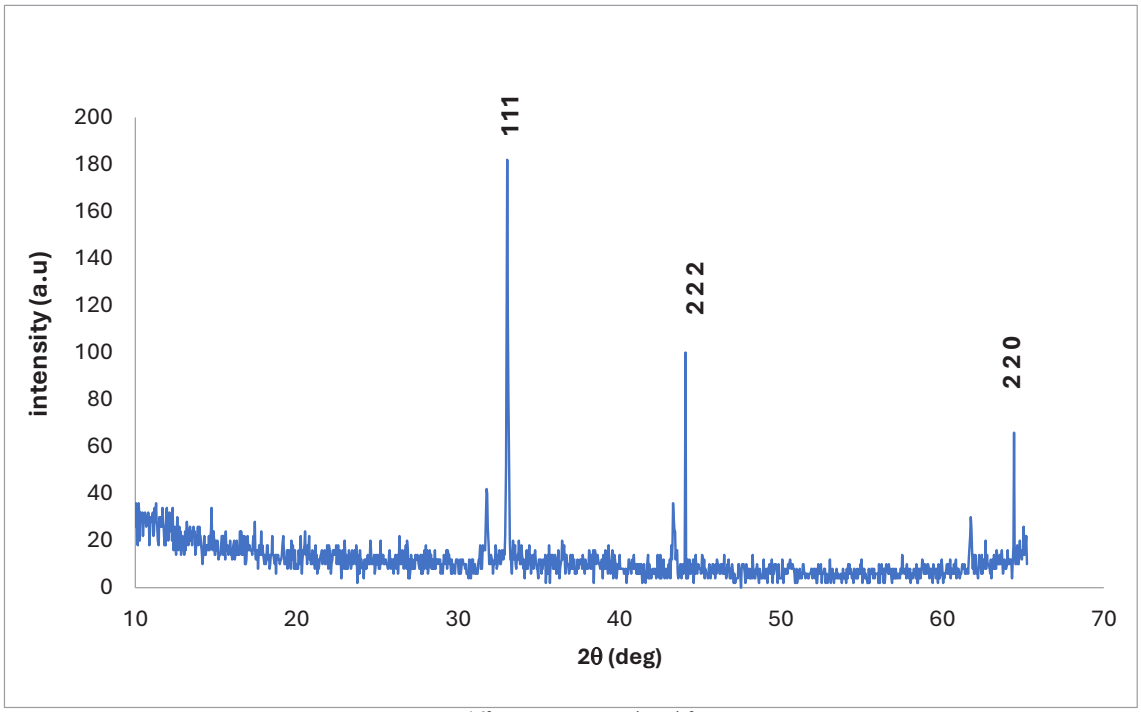

Fig. 1. X-ray diffraction patterns (XRD) for Au NPs.

irradiating the surface of the gold pellet with Nd:YAG laser energy (900 mJ, wavelength: 1065 nm) at a frequency of 1 Hz, gold nanoparticles were produced using laser ablation.

RESULTS AND DISCUSSION

X-ray diffraction test (XRD) X-ray diffraction

Samples obtained by using a Shimadzu 6000 X-ray diffractometer were analyzed for X-ray diffraction patterns (XRD) at a wavelength of λ = 1.54060 Å, at an applied voltage of 40KV. In Fig. 1, the XRD patterns of Au-NPs (laser-extraction method) generated with 900mJ of energy are presented. The characteristic peaks of the Au-NPs crystals (2θ = 38.39°, 44.75°65.96°, 77.84°) were found at (111), (200),(220), and (311) Miller indices, respectively, within an Fm-3m (space group No.225) crystal structure. The crystal's unit cell parameters were a=b,c=4.0699 Å, and unit cell angles were a=b=γ=90° which corresponds to the standard card [JCPDS 01-1172]. The reason for creating a cubic phase of gold nanoparticles at high-energy (900mj) laser illumination is due to the heat generated in the Au NPs from the laser. [16] To regulate the size of the nano-sized & crystal sized material and to check then different crystalline qualities of the nano based particles, the material was ablated using high energy. Since no new peaks were found, the Au-NPs produced have pure composition. Also, it can be concluded that all of the Au-NPs will continue to have cubic crystal phase during the complete derivative of the crystallization process. As shown in Fig. 1.

Uv-visible spectroscopy

UV-Visible spectroscopy is a method for determining the amount of light absorbed and scattered by a particular sample. The optical properties of a nanoparticle can be very useful for accurately determining its size, morphology (shape), concentration, and aggregate state. The UV-Visible spectrum of Au NPs produced at 900 mJ from a continuous pulse of 1000 pulses are shown in Fig. 2. The spectrum for Au NPs indicates that there is an absorption band at a specific wavelength, which corresponds with absorption bands that are typical for Au NPs. As a result of having mostly spherical particles in the suspension at this concentration, there was only one SPR peak found for the Au NPs. The peak of the Plasmon increased when the energy of the laser used for synthesis increased. The magnitude of the SPR peak depends on the concentration of particles in suspension, which means that as the concentration of particles increases, the amount of light that is absorbed also increases. [17,18].

The FTIR spectra for gold nanoparticles at different laser pulsed

The FTIR analysis of gold nanoparticles that were formed using a laser demonstrate observations of several peaks based primarily on

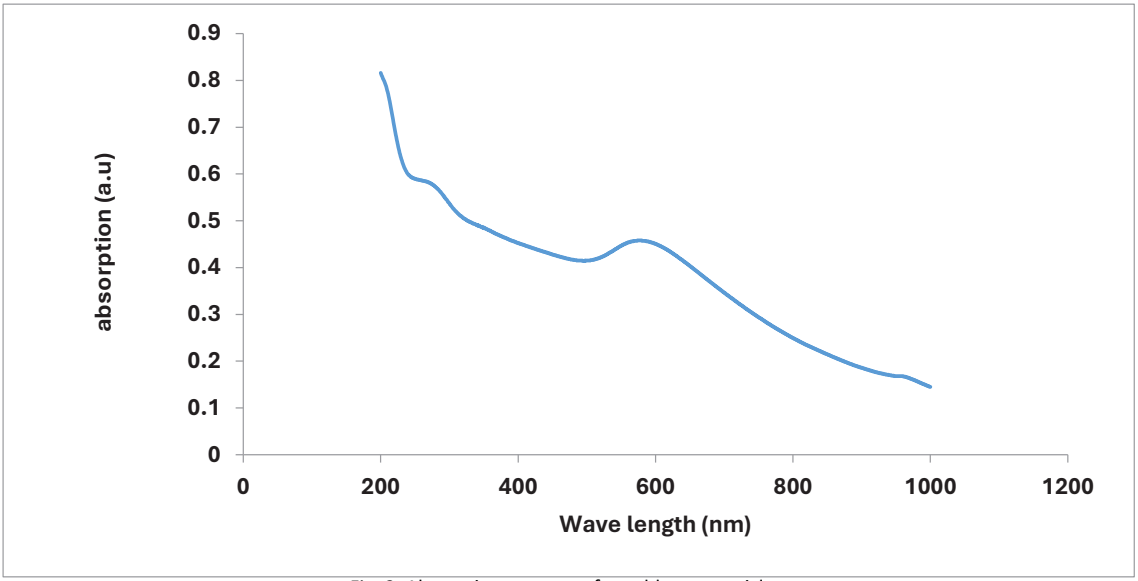

Fig. 2. Absorption spectrum for gold nanoparticles.

molecules that are coated onto the surface of the gold particles rather than based on the particle itself (as IR radiation cannot penetrate into your bulk gold particles). A very strong band located at (3400-3435 cm^{-1}) represents O-H stretching vibrations associated with the presence of water or hydroxyl groups that "stick" to the surface of the gold particles. Meanwhile, the peaks found between (2920-2850 cm^{-1}) are associated with C-H stretching vibrations as a result there exist residual organic material that has also stuck to the surface of the gold particles after synthesis. One of the most abundant peaks is observed at approximately (1633 cm^{-1}) which has been associated with H-O-H bending vibrations resulting from water molecules and/or the presence of carbonyl (C=O) bonds on

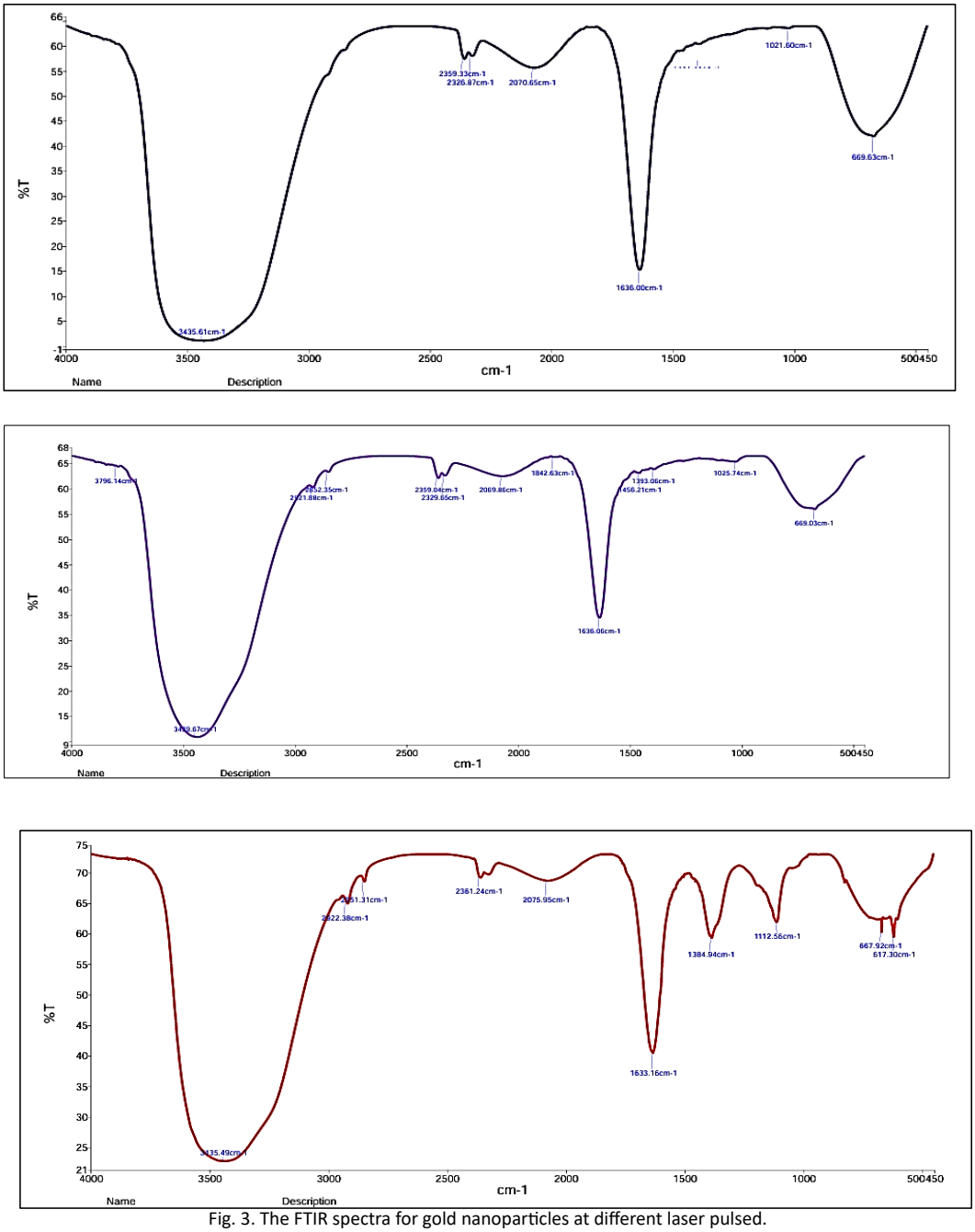

Fig. 3. The FTIR spectra for gold nanoparticles at different laser pulsed.

some of the organic materials also found on the surface of the gold nanoparticles. In addition to these observations the spectra will show the presence of numerous bands between (1380-1450 cm^{-1}) associated with C-H bending and/or COO- type building blocks, and bands between (1000-1120 cm^{-1}) associated with C-O or C-O-C stretching. (this is documented by Fig. 3). Also, the weaker interactions with an Au-O surface, as identified by its low frequency (600-670 cm^{-1}) band in the infrared region, may also lead to weak absorption features for many metallic-oxide interactions. These findings confirm that the produced gold nanoparticles are encapsulated with a layer of molecules that have been adsorbed through solution during laser ablation and play a significant role in stabilizing the nanoparticle and preventing the formation of aggregates. These findings support the successful synthesis, creation of chemically active and stable nanostructures.

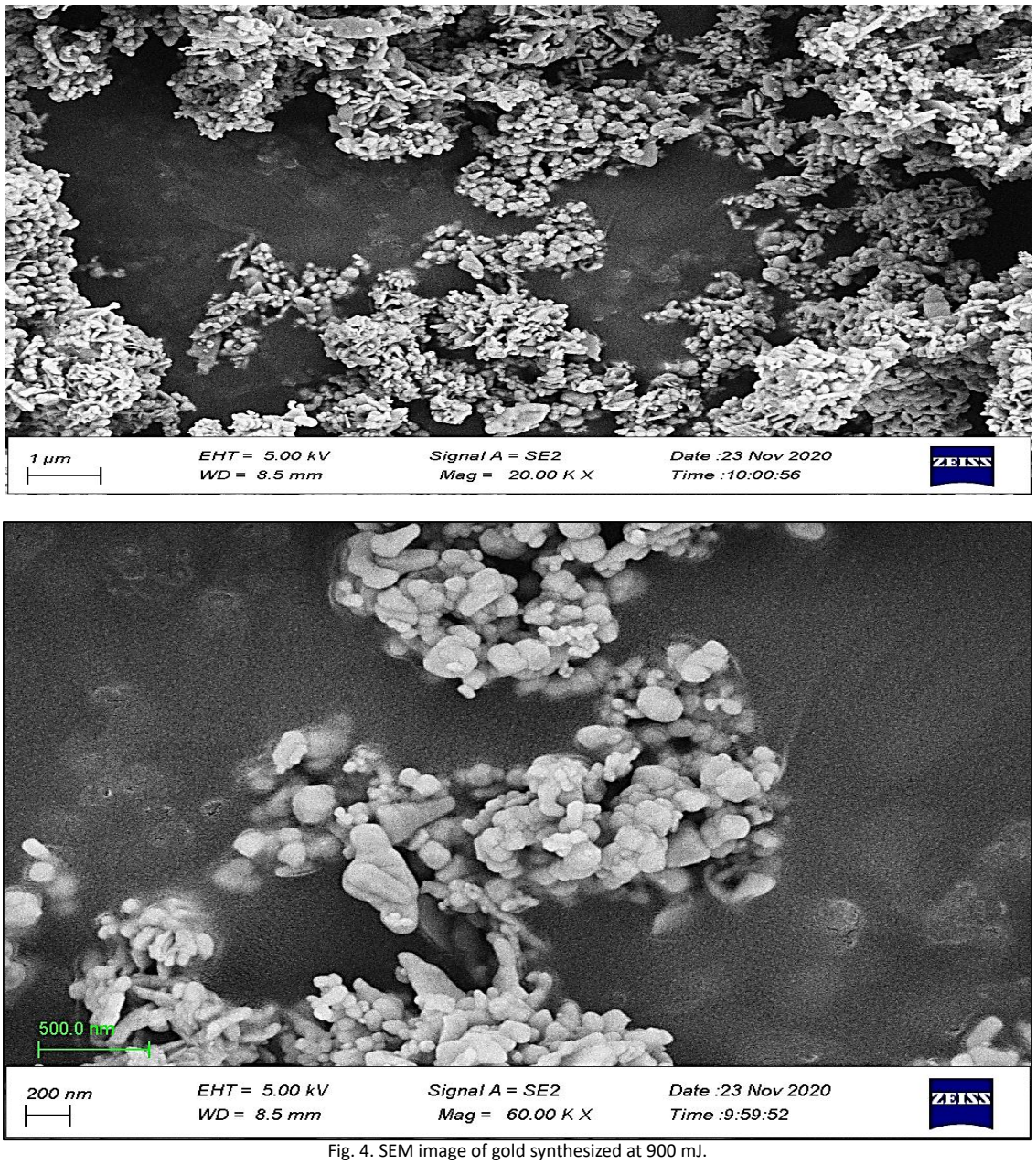

Fig. 4. SEM image of gold synthesized at 900 mJ.

[19].

Scanning electron microscopic for gold NPs

This scanning electron microscope (SEM) photograph of gold produced from laser energy at 900 mJ reveals a highly aggregated nanostructured morphology consisting of clusters of primary nanoparticles. These shapes resemble an irregular cauliflower-like aggregate with numerous small (tens of nanometers) approximately spherical full-globes bundled or fused together to create larger micron-scale clusters (see the bar in Fig. 4 for reference). Certain sites also exhibit characteristics similar to rods or platelets, implying some degree of anisotropic development amongst the more common spherical particles. The surface is rough and porous, resulting in a high surface area but also a considerable level of interaction and aggregate formation between neighbouring particles, most likely due to high levels of laser energy used for production. Overall, the contents of this image suggest that despite the relatively small size of the primary particles being measured at the Nano level, they are generally poorly dispersed and form dense, heterogeneous aggregates resulting from a small amount of colloidal stability, or a lack of stabilization of the primary particles during production.

Zeta Potentials

As demonstrated in Fig. 5, the zeta potential distribution has a distinct and prominent high value of zeta potential. Thus, the high zeta potential value indicates that the gold nanoparticles are very stable (high degree of electrostatic repulsion between particles) due to their strong electrostatic repulsion and, therefore, can remain well dispersed and not aggregate into larger particles [20]. The high +ve charge will also help promote better antibacterial efficacy of the gold nanoparticles due to enhanced binding to the negatively charged membranes of bacterial cells which will result in an increased ability of the nanoparticles to attach to and disrupt bacterial cells. Therefore, the zeta potential result above indicates the best condition for the gold nanoparticles to be stable and to have a good biological performance.

The electrophoretic mobility distribution of gold manufactured at a 900 mJ laser power setting has a distinct peak located at around +~3 µm. cm/V. s, showing that the majority of charged gold nanoparticles are very similar. The data is tightly distributed in a nearly Gaussian shape of approximately 2-4 µm/cm/V/s, indicating a low degree of polydispersity (small differences in sizes between the particles) and minimal aggregation (sticking together) due to relatively stable laser ablation conditions combined with sufficient energy to produce particles of nearly identical size without significant fragmentation. The large height of the peak represents a strong quality signal and a large concentration of similarly behaving particles. Thus, the 900 mJ laser synthesis conditions promote the formation of a very monodispersed and stable (due to electrostatic forces) gold nanoparticle suspension with little or no variability.

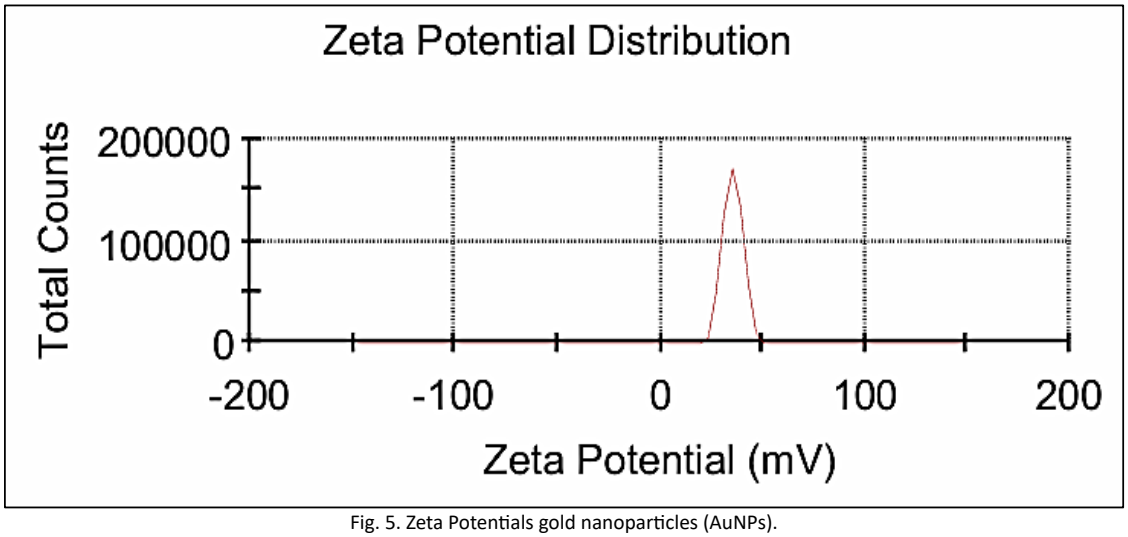

Fig. 5. Zeta Potentials gold nanoparticles (AuNPs).

Bacterial Samples Preparation

In this research, produced by researchers in Baghdad, are two types of bacteria, Escherichia coli (Gram negative) and Staphylococcus aureus (Gram positive), obtained from the Contaminated Bacteria Laboratory, Ministry of Science and Technology, Baghdad, Iraq. Using a sterile loop, one colony of each of the mentioned bacteria was inoculated into 10 ml of Nutritional Broth and incubated overnight (37 °C). After that, samples were then centrifuged for 5 minutes at 6000 RPM to form two types of bacterial solutions – Streptococcus (Gram +) at $1 - 10^8$ CFU/ml and E. coli (Gram -) at $1 - 10^8$ CFU/ml. After the supernatants

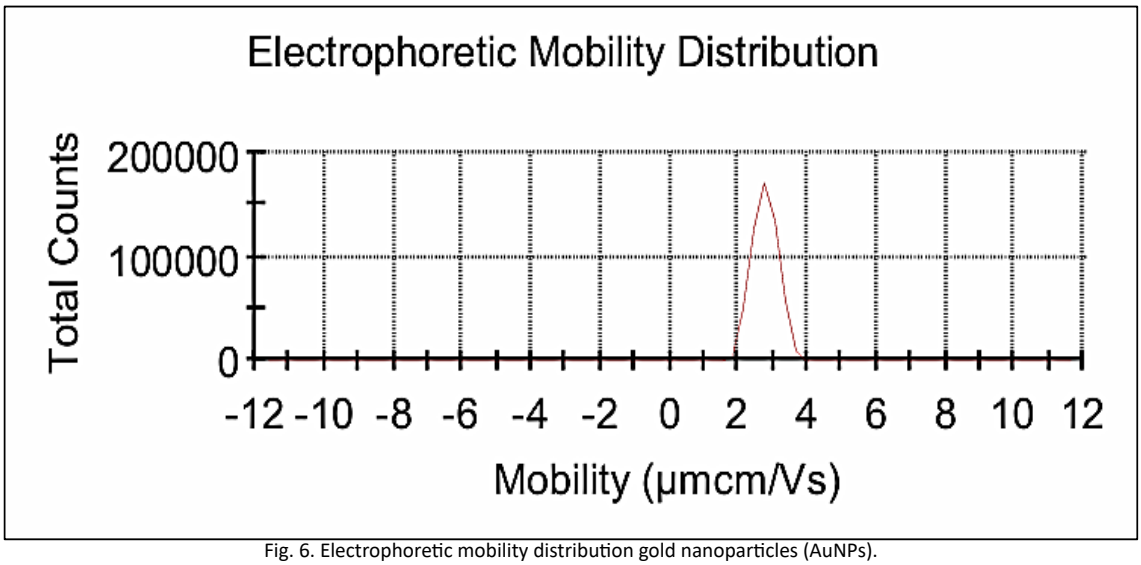

Fig. 6. Electrophoretic mobility distribution gold nanoparticles (AuNPs).

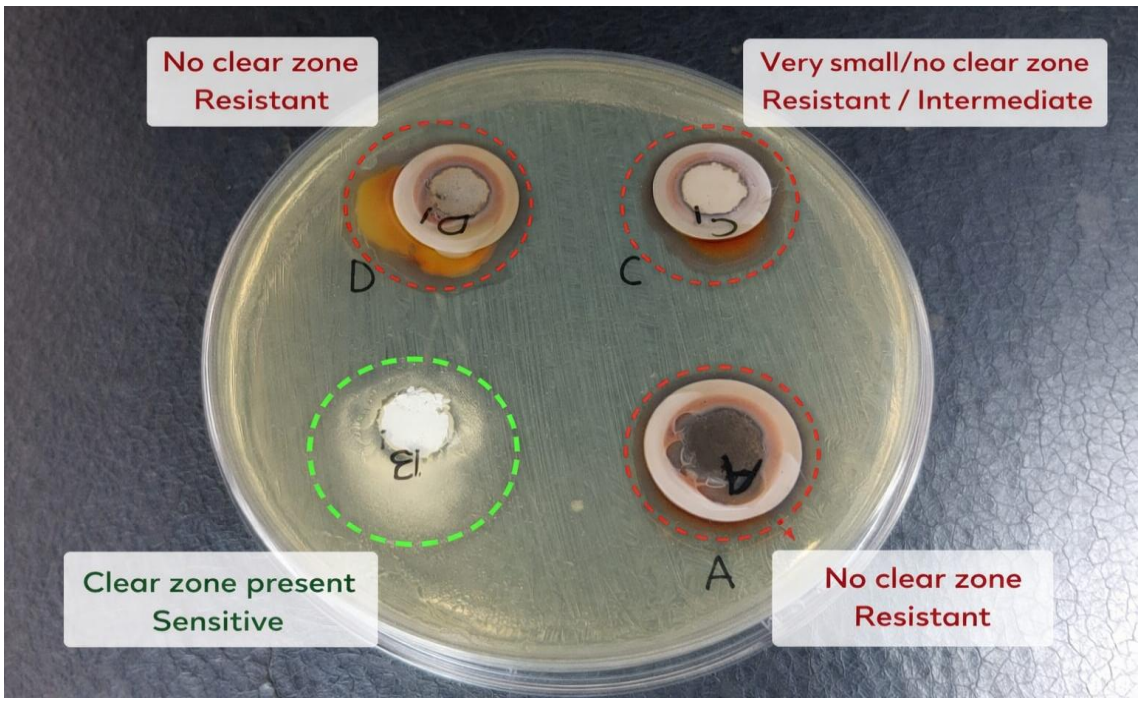

Fig. 7. Antibacterial activity of (Au NPs) against *S.aureus.* A, control. B, 25%. C, 50%. D, 75%. E, 100%.

were removed, the cells were resuspended in 500 µL of phosphate buffered saline (PBS) and then spun down three times to ensure all media and debris have been eliminated from the cells [21]. After removing the supernatant from the last wash, the cells were resuspended in 50 µL of PBS and pipetted to mix and ensure equal distribution of cells prior to placing them on the substrate. [22-24].

Antibacterial activity gold nanoparticles (AuNPs)

The Figs. 7 and 8 present a disk diffusion assay assessing the antibacterial activity of gold nanoparticles (AuNPs) against *Staphylococcus* species (likely *Staphylococcus aureus*) Bacterial inhibition testing showed that gold nanoparticles were effective against Staphylococcus and Escherichia coli as demonstrated by visible inhibition zones surrounding the discs infused with gold composites. This implies that gold nanoparticles have strong antibacterial activity (e.g., mechanisms such as disruption of bacterial cell membranes; oxidation of bacterial cells; disruption of other essential functions). The inhibition zone varied in size indicating the ability of gold nanoparticles against Staphylococcus; AuNPs

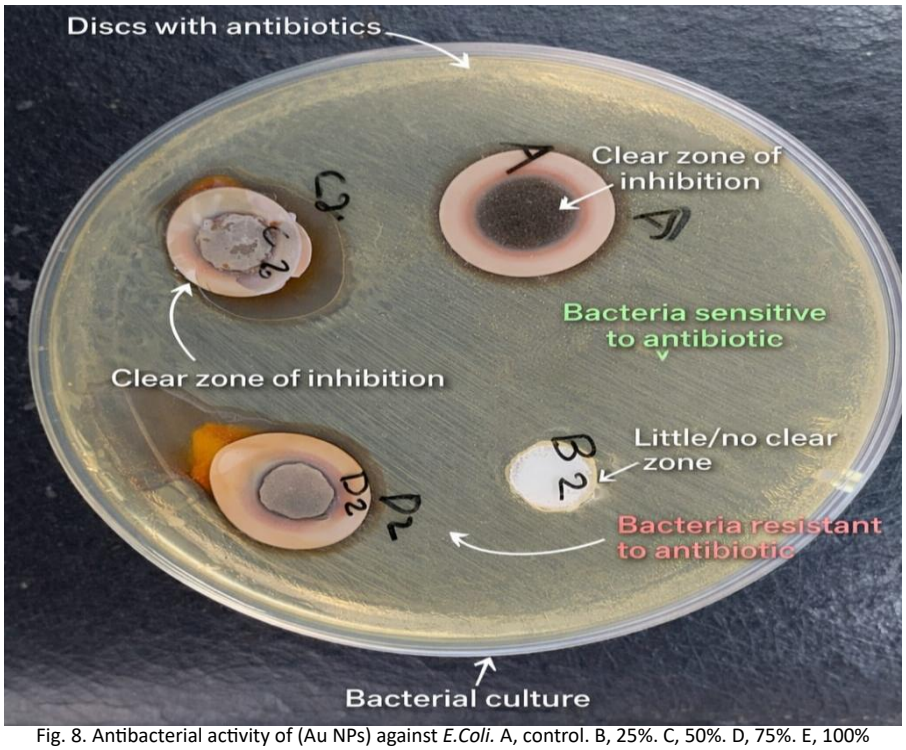

Fig. 8. Antibacterial activity of (Au NPs) against *E.Coli.* A, control. B, 25%. C, 50%. D, 75%. E, 100%

Table 1. Explain the antibacterial activity of nanoparticles.

	Antibacterial analysis (Zone of inhibition (mm))			
Sample	1	2	3	4
S.aureus	4	11	20	22
Au				
E.coli	5	9	18	21

likely disrupt bacterial cell membranes, increase membrane permeability, and form reactive oxygen species (ROS) that cause oxidative stress or destruction of essential biomolecules, including proteins, contributing to the observed antibacterial effect of AuNPs. AuNPs may also impede the intracellular activity of bacteria's enzymatic systems and lead to their subsequent death. Inhibition zones were variable indicating that several factors (e.g., particle size, concentration, surface characteristics) will affect the level of antibacterial potential of AuNPs [25,26].

Statistical analysis

Data were statically analysis using Graphpad prism program. Data are represented as mean ± SD of three experiments. Indicate statistically significant difference at $p < 0.05$.

CONCLUSION

Many studies have shown that copper and gold nanoparticles can be produced by using a variety of methods: chemical, physical and biological to name a few. The chemical and physical methods are extremely labor and time-intensive. Likewise, some of the chemical methods use toxic materials that can pose a health risk to the user. Thus, the development of rapid, affordable, environmentally-friendly methods is warranted. One approach for achieving this is through the use of biological methods for producing copper and gold nanoparticles. Research on the bioactivities of gold nanoparticles shown how well they worked against a variety of harmful bacteria, fungus.

CONFLICT OF INTEREST

The authors declare that there is no conflict of interests regarding the publication of this manuscript.

REFERENCES

1. Woźniak M, Płoska A, Siekierzycka A, Dobrucki LW, Kalinowski L, Dobrucki IT. Molecular Imaging and Nanotechnology—Emerging Tools in Diagnostics and Therapy. Int J Mol Sci. 2022;23(5):2658.
2. Kurul F, Turkmen H, Cetin AE, Topkaya SN. Nanomedicine: How nanomaterials are transforming drug delivery, bio-imaging, and diagnosis. Next Nanotechnology. 2025;7:100129.
3. Parthasarathy N, Karthikeyan L, Fabiola M, Vivek R. Recent progress in multifunctional theranostic inorganic nanomaterials for cancer diagnostic imaging and therapy. Next Nanotechnology. 2025;8:100212.
4. Nancy P, Nair AK, Antoine R, Thomas S, Kalarikkal N. In Situ Decoration of Gold Nanoparticles on Graphene Oxide via Nanosecond Laser Ablation for Remarkable Chemical Sensing and Catalysis. Nanomaterials. 2019;9(9):1201.
5. Hernández-Maya M, Rivera-Quintero P, Ospina R, Quintero-Orozco JH, García-Castro AC. Ablation energy, water volume and ablation time: Gold nanoparticles obtained through by pulsed laser ablation in liquid. Journal of Physics: Conference Series. 2019;1386(1):012062.
6. Alluhaybi HA, Ghoshal SK, Shamsuri WNW, Alsobhi BO, Salim AA, Krishnan G. Pulsed laser ablation in liquid assisted growth of gold nanoparticles: Evaluation of structural and optical features. Nano-Structures and Nano-Objects. 2019;19:100355.
7. Kuriakose AC, Nampoori VPN, Thomas S. Facile synthesis of Au/CdS core-shell nanocomposites using laser ablation technique. Mater Sci Semicond Process. 2019;101:124-130.
8. Saadoon AM, Al Gharawi M, Al-Mosawe A. Effect of Elevated Temperature on Microstructure and Mechanical Properties of Hot-Rolled Steel. Engineering, Technology and Applied Science Research. 2024;14(6):18756-18766.
9. Naharuddin NZA, Sadrolhosseini AR, Abu Bakar MH, Tamchek N, Mahdi MA. Laser ablation synthesis of gold nanoparticles in tetrahydrofuran. Optical Materials Express. 2020;10(2):323.
10. Saadoon NM, Hadi NM, Sabeeh SH. Diagnosis of copper plasma by laser induced breakdown spectroscopy. IOP Conference Series: Materials Science and Engineering. 2020;757(1):012023.
11. Daruich De Souza C, Ribeiro Nogueira B, Rostelato MECM. Review of the methodologies used in the synthesis gold nanoparticles by chemical reduction. J Alloys Compd. 2019;798:714-740.
12. Riedel R, Mahr N, Yao C, Wu A, Yang F, Hampp N. Synthesis of gold–silica core–shell nanoparticles by pulsed laser ablation in liquid and their physico-chemical properties towards photothermal cancer therapy. Nanoscale. 2020;12(5):3007-3018.
13. Kong F-Y, Zhang J-W, Li R-F, Wang Z-X, Wang W-J, Wang W. Unique Roles of Gold Nanoparticles in Drug Delivery, Targeting and Imaging Applications. Molecules. 2017;22(9):1445.
14. Simon J, Nampoori VPN, Kailasnath M. Facile synthesis of Au-Ag core shell and nanoalloy using femtosecond laser ablation and their optical characterization. Optik. 2019;195:163168.
15. Arvinte A, Crudu I-A, Doroftei F, Timpu D, Pinteala M. Electrochemical codeposition of silver-gold nanoparticles on CNT-based electrode and their performance in electrocatalysis of dopamine. J Electroanal Chem. 2018;829:184-193.
16. Khalil I, Julkapli N, Yehye W, Basirun W, Bhargava S. Graphene–Gold Nanoparticles Hybrid—Synthesis, Functionalization, and Application in a Electrochemical and Surface-Enhanced Raman Scattering Biosensor. Materials. 2016;9(6):406.
17. The Influence of ZnO NPs on Reproductive System Tissues of Albino Male Mice. Histopathological Study. International Journal of Science and Research (IJSR). 2017;6(7):2021-2025.
18. Chen Q, Ye Y, Liu J, Wu S, Li P, Liang C. Stability evolution of ultrafine Ag nanoparticles prepared by laser ablation in liquids. Journal of Colloid and Interface Science. 2021;585:444-451.
19. Menazea AA, Abdelghany AM. Precipitation of silver nanoparticle within silicate glassy matrix via Nd:YAG laser for biomedical applications. Radiat Phys Chem. 2020;174:108958.
20. Torrisi A, Cutroneo M, Torrisi L, Vacík J. Biocompatible

nanoparticles production by pulsed laser ablation in liquids. Journal of Instrumentation. 2020;15(03):C03053-C03053.
21. Jamaludin N, Chaudhary KT, Haider Z, Duralim M, Ismail FD, Roslan MS, et al. Effect of laser energy and wavelength on average size of gold nanoparticles synthesized by pulsed laser ablation in deionized water. Journal of Physics: Conference Series. 2020;1484(1):012029.
22. Staudinger U, Janke A, Simon F, Jakisch L, Bittrich E, Formanek P, et al. MWCNT Localization and Electrical Percolation in Thin Films of Semifluorinated PMMA Block Copolymers. Polymers. 2025;17(9):1271.
23. Comparison Study of Structural Properties and CO Adsorption on the Cu/Au(111) and Au/Cu(111) Thin Films. American Chemical Society (ACS). http://dx.doi.org/10.1021/acs.jpcc.8b04783.s001
24. alnada faris Husham K, khdier HM, Salih WM. Eco-friendly epoxy composites for high-performance skateboards. Discover Materials. 2025;5(1).
25. Mohammed MQ, Shugran AHM. Inhibitory effect of silver oxide nanoparticles and Saccharomyces cerevisiae on Escherichia coli and Staphylococcus aureus bacteria. Experimental and Theoretical NANOTECHNOLOGY. 2026;10(1):13-23.
26. Rahmah MI, Saadoon NM, Mohasen AJ, Kamel RI, Fayad TA, Ibrahim NM. Double hydrothermal synthesis of iron oxide/silver oxide nanocomposites with antibacterial activity **. Journal of the Mechanical Behavior of Materials. 2021;30(1):207-212.